ACS SyntheticBiology

pubs.acs.org/synthbio

Research Article

A Simple Biosensor-Based Assay for Quantitative Autoinducer-2 Analysis

Marla Keizers, Ulrich Dobrindt,* and Michael Berger*

Cite This: *ACS Synth. Biol.* 2022, 11, 747−759

Read Online

ACCESS | Metrics & More | Article Recommendations | Supporting Information

ABSTRACT: Bacteria produce and react to interspecies signaling molecules in order to control the expression of genes that are particularly beneficial when they are expressed by a bacterial community. In addition to intraspecies communication, the signaling molecule autoinducer-2 (AI-2) can also serve for interspecies communication between Gram-positive and Gram-negative bacteria and is therefore of particular interest. The analysis and quantification of AI-2 are essential for understanding population density-dependent changes in bacterial behavior and pathogenicity. However, currently available bioassays for AI-2 quantification are rather complex, have narrow detection ranges, and are very sensitive to trace components of, for example, growth media. To facilitate and improve the detection of AI-2, we have developed an *Escherichia coli* biosensor-based assay that is sensitive, cheap, fast, robust, and reliable in the quantification of biologically active AI-2. The bioassay is based on an *lsr* promoter-fluorescent reporter gene fusion cassette that we chromosomally integrated in a biosensor strain, but the cassette can also be used in a low-copy number plasmid for the application in other Gram-negative bacterial species. We show here that AI-2 quantification was possible in a concentration range from 400 nM to 100 μM and that a critical interpretation of the kinetics of the measurements can reveal sugar interference. With the help of our biosensor strain, coculture experiments were done to test the capability and kinetics of AI-2 secretion by various Gram-negative bacteria in real time. Finally, calibration curves were used to calculate the absolute AI-2 concentration in cell-free bacterial samples.

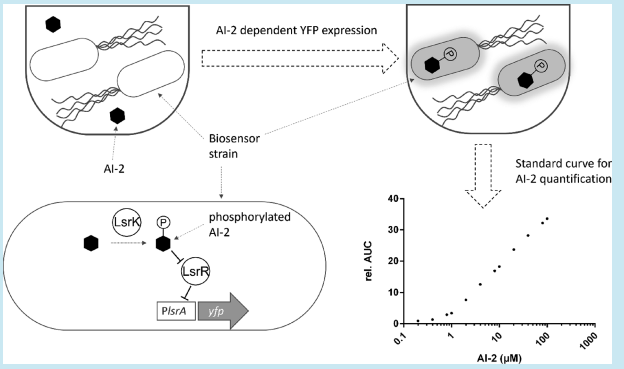

KEYWORDS: *biosensor, autoinducer-2, real-time detection, quantification bioassay, fluorescence, quorum sensing*

INTRODUCTION

The coordination of population density-dependent gene expression in bacteria is referred to as quorum sensing (QS).[1] QS is usually employed in order to control genes that are particularly beneficial when they are expressed by a bacterial community rather than by a single bacterium, e.g., genes that are involved in biofilm formation or virulence.[2−5] Among others, AI-2 is known to be an essential universal interspecies signaling molecule. Its precursor, (*S*)-4,5-dihydroxy-2,3-pentanedione (DPD), is synthesized as a byproduct of L-homocysteine production by the synthase LuxS,[6] a widely distributed enzyme among Gram-positive and Gram-negative bacteria.[7] Depending on the environmental status, DPD spontaneously circularizes to either boron-containing (*S*)-2-methyl-2,3,3,4-tetrahydroxytetrahydrofuran-borate (S-THMF-borate)[8] or boron-free (*R*)-2-methyl-2,3,3,4-tetrahydroxytetrahydrofuran (R-THMF).[9] The quick interconversion of AI-2 enables interspecies bacterial crosstalk since both products are sensed by different kinds of receptors.[2,8−12] Apart from LuxS-dependent DPD generation, there is evidence for LuxS-independent AI-2 synthesis,[13] as well as for AI-2 mimicking molecules that are produced by eukaryotic cells.[14] The most well-characterized AI-2 receptors are the periplasmic binding proteins LuxP, binding S-THMF-borate,[8] and LsrB, binding R-THMF.[9] LuxP has so far only been found in *Vibrio* spp.[5,7,15] In response to AI-2, *Vibrio* spp. produce bioluminescence by a signaling cascade involving the sensor kinase/phosphatase LuxQ.[8,15] LsrB, on the other hand, was found to be part of an AI-2 import system.[16] The receptor was first described in the Gram-negative bacterium *Salmonella enterica* serovar Typhimurium (*S.* Typhimurium)[16] and was later also found to be expressed by the enteric bacterium *Escherichia coli* (*E. coli*)[17] as well as by several other bacteria.[5,18] After the import, AI-2 is phosphorylated by the kinase LsrK.[16,19] The phosphorylated AI-2 inactivates LsrR, a transcription factor that represses the expression of the *lsrRK* and the *lsrACDBFG* operons (Figure 1).[19,20] In addition to that, the expression of the *lsrRK* and the

Received: September 16, 2021
Published: January 28, 2022

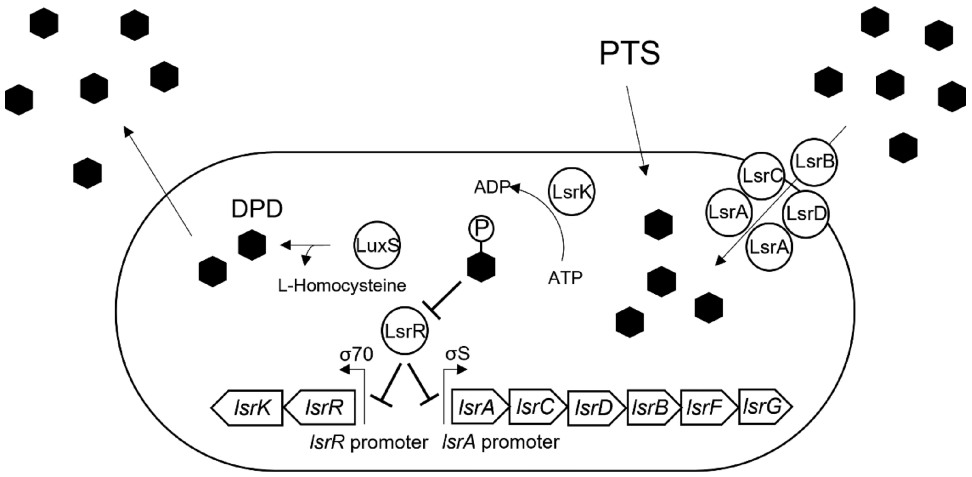

Figure 1. Schematic model of AI-2-dependent *lsr* operon expression in *E. coli*. DPD, the precursor of biologically active AI-2, is synthesized as a byproduct of L-homocysteine production via LuxS[6] and transported out of the cell since it is hydrophilic and thus considered to be membrane-impermeable.[25] As the extracellular AI-2 concentration increases, the molecule is initially transported back into the cell by a PTS-dependent mechanism.[26] Upon incorporation, AI-2 is phosphorylated by LsrK[16,19] and subsequently inactivates the *lsr* operon repressor LsrR.[19,20] *LsrA*-promoter induction leads to the expression of the Lsr ABC-transporter (LsrA, LsrB, LsrC, and LsrD) resulting in a quick internalization of extracellular AI-2.[16−18] Phosphorylated AI-2 is afterward degraded by LsrF and LsrG.[27]

lsrACDBFG operons is also strictly regulated by catabolite repression. Therefore, both operons are only expressed when they are simultaneously activated by CRP-cAMP.[17,20,21] Apart from LsrB and LuxP, also, the periplasmic receptor RbsB, which is part of a ribose import system and shows structural similarities to LuxP,[8] is known to function synergistically in AI-2 uptake with LsrB in *Aggregatibacter actinomycetemcomitans* JP2 and *Yersinia pestis* CO92 or LsrB-independent in the nontypeable *Haemophilus influenzae* strain 86-028NP.[22−24]

Several bioassays have been described for the qualitative or quantitative AI-2 analysis in bacterial culture supernatants. Table S1 of the Supporting Information shows a list of these assays, including their advantages and limitations (Table S1).

The most widely used AI-2 bioassay is a bioluminescence assay based on *Vibrio harveyi* (*V. harveyi*) strains that produce light in response to AI-2.[4,15] Two genetically engineered *V. harveyi* strains are mostly used. Both strains lack the protein LuxN (*luxN*::*tn5*) and therefore do not produce light in reaction to autoinducers other than AI-2. The first strain is *V. harveyi* BB170, which produces AI-2 as the population grows,[15] and the second strain is *V. harveyi* MM32, which is unable to synthesize AI-2 due to a *luxS* deletion.[9] According to the literature, quantitative dose−response curves range between 0.1 nM and 800 nM in *V. harveyi* BB170[14,28,29] and between 1 nM and 5 μM in *V. harveyi* MM32,[30−32] which makes these strains sensitive detectors of low amounts of borated AI-2 (BAI-2). However, AI-2 concentrations above 35 μM show a bioluminescence quenching effect.[28] In addition, Vilchez et al. showed that growth and bioluminescence of *V. harveyi* were strongly influenced by trace elements, which can directly inhibit AI-2 detection.[28] Another problem is that boron is, on the one hand, essential for the assay but, on the other hand, can lead to false-positive results at concentrations higher than 500 μM.[28] A similar problem is known for the very common media component glucose that can inhibit luminescence and lead to false-negative results[28,33] but can also lead to false-positive results at concentrations higher than 0.08 g/L.[34] Long et al. generated a *V. harveyi* reporter strain that is, due to *luxN*/*cqsS*[35] mutations, also restricted to AI-2-dependent induction of luminescence and, due to a *luxS* deletion, unable to synthesize AI-2.[6,36] In this strain, the open reading frame of the green fluorescent protein (GFP) was transcriptionally fused to the *qrr4* promoter that is activated by LuxO-P via the BAI-2-binding LuxP receptor.[36,37] In a single-cell assay, the strain detected BAI-2 in the range of 1 nM−1 μM, thus being as sensitive as the bioluminescent reporter. An additional method for detecting AI-2 is an in vitro FRET approach. The assay uses a LuxP receptor protein coupled to a cyan fluorescent protein (CFP) and a yellow fluorescent protein (YFP). Upon BAI-2 binding, a change in fluorescence resonance energy transfer between the fluorescent proteins can be detected in the range between 1 μM and 60 μM.[38,39] Noteworthy, the detection range can vary between protein batches,[39] and the observed overall FRET signal change was very small.[40] In addition to LuxP, also, an LsrB-based biosensor was constructed. The LsrB-based assay shows a linear range in between 20 μM and 2 mM AI-2.[40] However, this assay requires additional fluorescent dyes that are costly and not always commercially available.[39]

Another prevalent AI-2-dependent QS screening technique is the usage of *lsrA*-promoter fusions with *lacZ* in either *E. coli*[32,41,42] or *V. harveyi*.[43,44] A subsequent β-galactosidase activity assay then enables the quantification of AI-2 in concentrations of more than 1000 μM.[32] However, even though there are several described modifications of β-galactosidase assays that allow single-step[45] and 96-/384-plate-based[42] protocols, the assay is time-consuming and error-prone due to multiple downstream steps. Here, we describe a simple *E. coli* biosensor-based assay for a sensitive quantitative AI-2 analysis. We tested an *E. coli lsrRK lsrA* promoter-*yfp* fusion reporter module that was either chromosomally integrated in the phage λ attachment site (*attB*::P*lsrA-yfp*) or on a low-copy plasmid (pMK1) in an *E. coli* K-12 MG1655 *luxS* mutant background (*E. coli* Δ*luxS*). We show that using this simple assay, the quantification of extracellular DPD/AI-2 concentrations in between 400 nM and 100 μM was possible. In addition, sugars in analyzed samples were clearly detectable by analyzing the kinetics of the module response. In addition to AI-2 quantification, the reporter module can be used for real-time AI-2 determination by mixing a bacterial strain to be tested with the biosensor strain *E. coli* Δ*luxS* with the

https://doi.org/10.1021/acssynbio.1c00459
ACS Synth. Biol. 2022, 11, 747−759

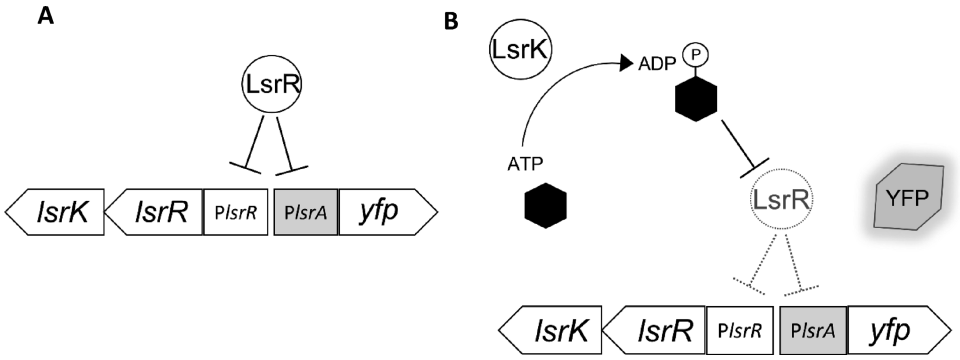

Figure 2. Reporter construct for the measurement of AI-2-dependent YFP expression. (A) The module comprises the *E. coli lsrRK* operon and *yfp* coupled to the *E. coli lsrA* promoter. The expression of YFP is therefore repressed by LsrR. (B) As soon as extracellular AI-2 is incorporated, basal levels of LsrK phosphorylate AI-2 that subsequently represses LsrR. The AI-2-dependent repression of LsrR results in AI-2-dependent YFP expression.

chromosomally integrated module (*E. coli* Δ*luxS* (*attB*::P*lsrA-yfp*)). Taken together, our *E. coli* Δ*luxS* (*attB*::P*lsrA-yfp*) biosensor, as well as pMK1, offer new opportunities for an easy, fast, and reliable AI-2 quantification and kinetic screening.

RESULTS AND DISCUSSION

Construction of the P*srA* Module. To overcome the limitations of currently used bioassays for AI-2 quantification, we developed a reporter gene construct that allows for real-time quantification of biologically active AI-2. As already mentioned, the Lsr ABC transporter is the best described AI-2 uptake system in enteric bacteria and members of other bacterial families (Figure 1).[2,5] Its receptor LsrB is part of the system that, upon activation, quickly depletes extracellular AI-2.[16−18] We chose the *lsrA* promoter (P*lsrA*) for our reporter module (Figure 2) because its activation is directly dependent on LsrR suppression by phosphorylated AI-2 (Figure 2B).

Our P*lsrA* module, therefore, makes direct use of the intracellular AI-2 phospho-AI-2 circuit.[19,20] The construct is depicted in Figure 2A and comprises the P*lsrA-yfp* transcriptional fusion, as well as a resistance marker (*cat*; not shown in the scheme) directly downstream of *yfp*. In addition, the module comprises *lsrR and lsrK*, as the higher background transcription levels of less complex, ectopically integrated reporter constructs were previously attributed to the lack of these regulators.[19] The original P*lsrA-yfp* fusion was constructed in the chromosome of the *E. coli* K-12 strain MG1655 (*E. coli*) and then cloned in the low-copy vector pWKS30, and the resulting plasmid was named pMK1. The plasmid was introduced in *E. coli* Δ*luxS*, and we named the strain harboring pMK1 *E. coli* Δ*luxS* (pMK1). In addition, the module was integrated in the phage λ attachment site (*attB*) (reviewed in ref 46) for direct use as a biosensor. The *attB* site was chosen as an integration site because the *attB* site and its flanking regions are highly conserved, thus facilitating the potential future transfer of the module in other *E. coli* isolates by recombineering. With respect to the regulation of the module, the *attB* site was expected to be as neutral as any other sites of the *E. coli* chromosome.[47] We named the resulting strain carrying the chromosomally integrated reporter module *E. coli* Δ*luxS* (*attB*::P*lsrA-yfp*). Like in its native locus, LsrR represses *lsrRK* and P*lsrA*-dependent YFP expression (Figure 2A). After internalization, external AI-2 is phosphorylated by the LsrK kinase and is therefore repressing LsrR. The repression of LsrR then results in the induction of YFP expression via P*lsrA* (Figure 2B).[19] The YFP was chosen because it provides a high and stable fluorescence signal that can also easily be detected in real time when expressed from chromosomally integrated modules.[47] By choosing the *E. coli* intracellular AI-2 phospho-AI-2 circuit, our module directly depends on gene regulation by LsrR.[19,20] Also, in addition to the *lsrA* and *lsrR* operons, LsrR also represses genes related to virulence traits in *E. coli* and *S.* Typhimurium.[48,49] Therefore, an LsrR-repressed reporter module could also serve as indirect evidence for general gene activation due to biologically active AI-2 incorporation. Recently, an sfGFP-based two-plasmid system utilizing the same AI-2 phospho-AI-2 circuit was described, but its usefulness for absolute quantification of AI-2 in biological samples was not tested.[50,51] Notably, using this circuit, the screening for BAI-2 might still require conversion of BAI-2 in boron-free AI-2 since the widely described uptake mechanism receptor LsrB binds only to nonborated AI-2.[9,18] In addition, the negative charge in LsrB makes it unlikely that BAI-2 is imported into the cell via LsrB.[9] Nevertheless, the LsrB-independent incorporation of BAI-2, eventually via sugar transporters, remains to be investigated.

Tests for Function and Specificity. First, we tested our module in *E. coli* Δ*luxS* (pMK1) according to the assay protocol (a detailed step-by-step protocol is provided in the Supporting Information) for functionality and specificity. We tested synthetic DPD (10 μM final concentration) and the cell-free supernatant of *E. coli* as well as the cell-free supernatant of the *E. coli* Δ*luxS* mutant after 6 h of growth in LB broth (Figure 3A,B). Upon addition of synthetic DPD or wild-type *E. coli* cell-free supernatants, we saw a fluorescence signal (depicted as relative fluorescence units, RFU), whereas the addition of H_2O or the Δ*luxS* mutant cell-free supernatant only led to a very low but detectable background fluorescence signal (Figure 3A,B). This indicated that the reporter module was indeed specifically induced by AI-2, irrespective of whether it was naturally or synthetically produced. The promoter kinetics, depicted as the first derivative of the RFU kinetics (promoter activity), revealed maximal promoter induction 70−80 min after addition of 10 μM synthetic DPD and 90 min after the addition of the *E. coli* cell-free supernatant (Figure 3C). To calculate the promoter induction strength, we calculated the areas under the curve of the promoter induction kinetics. Within every kinetics, the largest area under the curve measurement was further used as an assay measuring unit and

https://doi.org/10.1021/acssynbio.1c00459
ACS Synth. Biol. 2022, 11, 747−759

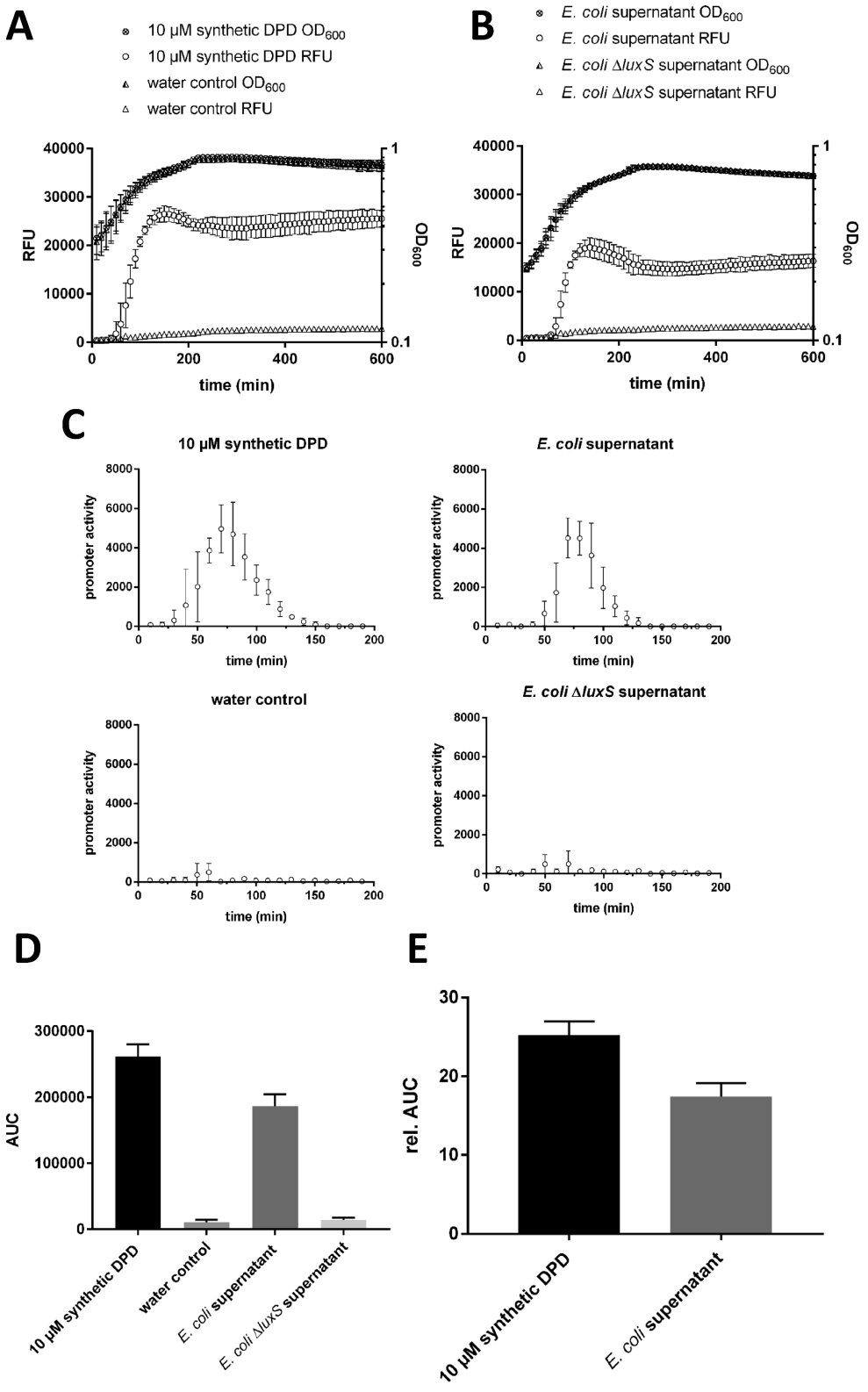

Figure 3. Functional test of the reporter module. Relative fluorescence (RFU) and optical density (OD_{600}) kinetics of *E. coli* Δ*luxS* (pMK1). (A) Kinetics upon addition of 10 μM synthetic DPD and H_2O (sample volumes of 10 μL) and (B) *E. coli* cell-free supernatant after 6 h of growth and *E. coli* Δ*luxS* cell-free supernatant after 6 h of growth (sample volumes of 50 μL). (C) Promoter induction depicted as promoter activity. (D) AUC calculation of promoter inductions. (E) Relative AUC of the indicated treatment to the control (water or *E. coli* Δ*luxS* cell-free supernatant). The total assay volume was 200 μL. Error bars represent three biological replicates.

shortly named as AUC (Figure 3D). In order to correct for background level expression of the module, we calculated the ratio of the AUC of samples to the AUC of the corresponding negative control (rel. AUC). We saw a 25-fold induction of the module upon addition of 10 μM synthetic DPD and a 17-fold induction of the module upon addition of *E. coli* cell-free

https://doi.org/10.1021/acssynbio.1c00459
ACS Synth. Biol. 2022, 11, 747−759

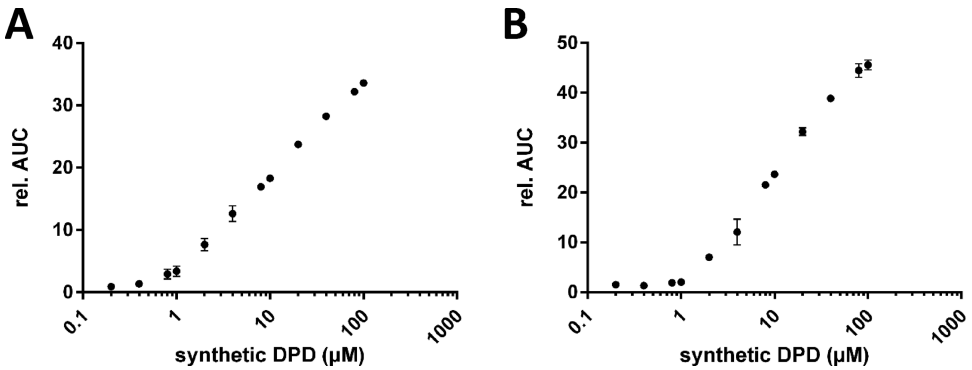

Figure 4. Dose−response curves of the P*lsrA* modules shown as synthetic DPD concentration-dependent relative AUC measurements. Relative AUC of (A) *E. coli* Δ*luxS* (pMK1) or (B) *E. coli* Δ*luxS* (*attB*::P*lsrA-yfp*) in reaction to different synthetic DPD concentrations. Added concentrations were 100 μM, 80 μM, 40 μM, 20 μM, 10 μM, 8 μM, 4 μM, 2 μM, 1 μM, 800 nM, 400 nM, and 200 nM as well as H_2O as a negative control. Sample volumes were 10 μL in each case. The total assay volume was 200 μL. Error bars represent one biological replicate with three technical replicates.

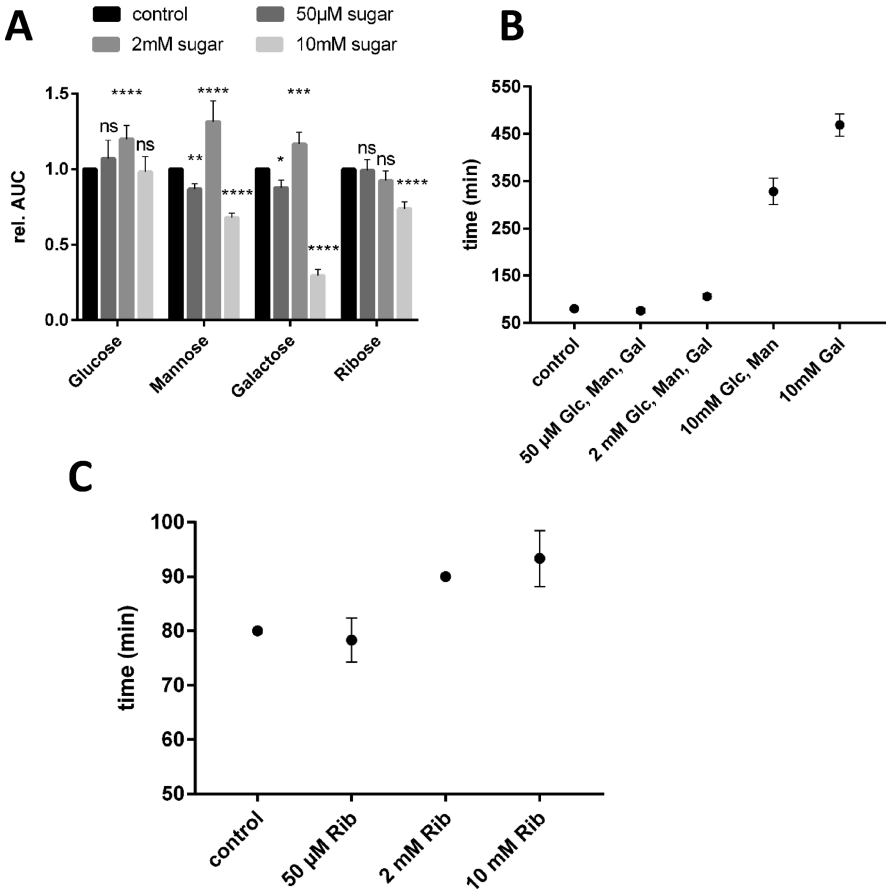

Figure 5. Sugar effect on the induction of the AI-2-dependent YFP expression. (A) Induction of the P*lsrA* module of *E. coli* Δ*luxS* (pMK1) depicted as relative AUCs in the presence of different sugars. Shown is the relative AUC of samples with 10 μM synthetic DPD supplemented with the indicated sugar concentrations. $AUC^{control}$ was 10 μM synthetic DPD only. Sample volumes were 10 μL in each case. The total assay volume was 200 μL. Statistical analysis was performed using two-way ANOVA; values <0.05 are considered statistically significant. (B) Time points of maximal P*lsrA* induction upon addition of 10 μM synthetic DPD supplemented with H_2O (control); 50 μM Glc, Man, or Gal; 2 mM Glc, Man, or Gal; and 10 mM Glc or Man. Upon addition of 10 mM Gal, only the second time point of P*lsrA* induction is depicted. (C) Time point of maximal P*lsrA* induction upon addition of 10 μM synthetic DPD supplemented with H_2O (control), 50 μM Rib, 2 mM Rib, and 10 mM Rib. Error bars represent three biological replicates with two technical replicates each.

supernatant (Figure 3E). These results show (i) that synthetically as well as biologically produced AI-2 are inducers of our module and (ii) that our module is specifically induced by AI-2, as adding the culture supernatant of *E. coli* Δ*luxS* was equivalent to adding water to our biosensor, indicating that it did not contain components that were interfering with our assay.

Determination of the Linear Range of the Measurement. Next, we tested both the pMK1-based and the chromosomal *attB*::P*lsrA-yfp* reporter construct regarding the

https://doi.org/10.1021/acssynbio.1c00459
ACS Synth. Biol. 2022, 11, 747−759

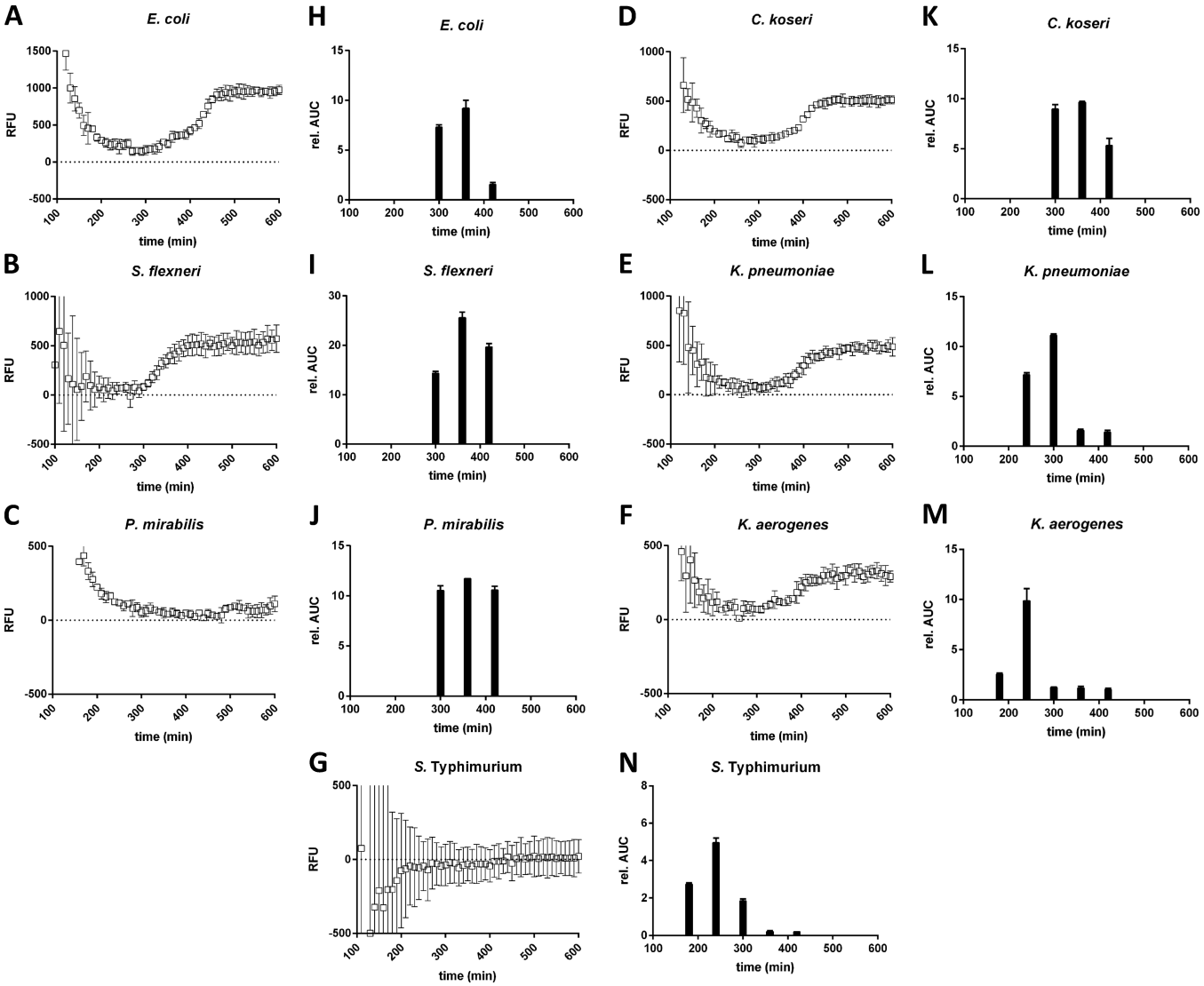

Figure 6. Comparison of AI-2 production kinetics by different enterobacterial isolates. (A–G) Fluorescence kinetics (100–600 min), depicted as RFU, during coculture with *E. coli* Δ*luxS* (*attB*::P*lsrA-yfp*) and (A) *E. coli*, (B) *S. flexneri*, (C) *P. mirabilis*, (D) *C. koseri*, (E) *K. pneumoniae*, (F) *K. aerogenes*, and (G) *S.* Typhimurium. The total assay volume was 200 μL. Error bars represent three biological replicates. (H–N) Relative AUC measurements of cell-free supernatants at the indicated time points during monoculture of (H) *E. coli*, (I) *S. flexneri*, (J) *P. mirabilis*, (K) *C. koseri*, (L) *K. pneumoniae*, (M) *K. aerogenes*, and (N) *S.* Typhimurium. $AUC^{control}$ was *E. coli* Δ*luxS* cell-free supernatant. Sample volumes were 50 μL in each case. The total assay volume was 200 μL. Error bars represent three technical replicates.

linearity of our AI-2 concentration measurements. We saw that the strength of the module induction correlated very well with AI-2 concentration, i.e., resulting in higher AUC with increasing DPD concentrations (Figure S1). We were able to generate highly reproducible dose–response curves in a range between 400 nM and 100 μM of the synthetic DPD final concentration by using pMK1 (Figure 4A) and in a range between 1 μM and 100 μM of the final concentration by using the chromosomal reporter fusion (Figure 4B). Figure 4 shows average values and standard deviations of one experiment with three technical replicates. The absolute fluorescence emission differed more in between biological replicates than in between technical replicates of one experiment. However, the relative strength of promoter induction in response to increasing AI-2 concentrations remained reproducible (see Figure S2A,B for two additional biological replicates). This was expected and simply shows that a standard curve with known inducer concentrations is necessary for absolute quantifications, whereas the relative quantification of the AI-2 concentrations in two samples is easily possible without a standard curve.

Sensitivity of the Modules to Sugar Interference. As already shown above, the module was not activated in the culture supernatant of *E. coli* Δ*luxS*, indicating that it is specific for AI-2. However, it is well-known that especially, the bioluminescence-based *V. harveyi* AI-2 detection assay is strongly susceptible to sugar, leading to false-positive or false-negative results, which is especially problematic, as AI-2 quantification is often done in culture supernatants.[28,34] Turovskiy and Chikindas showed that glucose traces of 0.08 g/L led to a 20-fold induction of bioluminescence, whereas residues of 2 g/L nearly completely quenched bioluminescence.[34] Also, the expression of the *E. coli lsr* operon is known to be negatively affected by sugars, e.g., by CRP-mediated carbon catabolite repression via glucose or glycerol[17,21] or by direct regulation of LsrK via HPr, a protein that is part of the

https://doi.org/10.1021/acssynbio.1c00459
ACS Synth. Biol. 2022, 11, 747–759

phosphoenolpyruvate-dependent sugar phosphotransferase system (PTS).[52]

We therefore systematically tested the effect of different sugars on the induction of P*lsrA* in *E. coli* Δ*luxS* (pMK1). We added different amounts of D-(+)-glucose (Glc), D-(+)-mannose (Man), D-(+)-galactose (Gal), and D-(−)-ribose (Rib) to a fixed amount of DPD (10 μM) and determined the relative AUC according to the assay protocol (Figure 5A). For the subsequent analysis, we used the AUC of 10 μM DPD with no sugar supplementation as a control. When compared to the control, we saw in between 0.9-fold suppression and 1.1-fold induction upon addition of 50 μM sugar, in between 0.9-fold suppression and 1.3-fold induction upon addition of 2 mM sugar, and a suppression up to 0.3-fold at 10 mM, depending on the type of sugar (Figure 5A).

Interestingly, the effect of Glc, Man, or Gal supplementation was clearly discernible in the promoter kinetics. Without addition of any sugar, the module was maximally induced after 70−80 min, and the induction kinetics of the module was very similar to the kinetics for 50 μM for all sugars (Figure 5B,C and Figure S3). However, upon addition of 2 mM Glc, Man, or Gal, the module showed a weak induction after approximately 70 min followed by a transient decline in activity and a second peak after approximately 100 min (Figure S3A−C). Therefore, the higher total YFP expression, as compared to addition of none or 50 μM sugar, was not due to a higher YFP expression rate but an overall longer response of the module (compare Figure 5A to Figure S3A−C). Upon addition of 10 mM Glc or Man, the module again showed a weak induction after 70 min, similar to what we observed upon supplementation of 2 mM of the same sugars. However, the second peak was substantially delayed for approximately 3.5 h (Figure 5B and Figure S3A,B). The addition of 10 mM Gal had a similar effect, but the second peak was even more delayed than that for Glc and Man. Moreover, the YFP production rate was also reduced, most likely due to AI-2 instability.[53,54] As the second peak was also substantially smaller than that with a lower or no Gal supplementation, the AUC was significantly lower upon supplementation of 10 mM Gal (compare Figure S3C to Figure 5A). The observed activity pattern of the module in the presence of Glc, Man, and Gal could be explained by a coordinated interplay of the regulators of P*lsrA*: The first peak likely resulted from LsrR-AI-2-dependent de-repression of the promoter. However, the transient or longer-lasting decline of promoter activity is most likely due to the lack of CRP-dependent promoter activation due to a sugar-dependent drop in cAMP levels. Glc and Man are PTS-dependent sugars, and uptake via PTS results in a low intracellular cAMP level (reviewed in refs 55−57). Gal, on the other hand, is transported via GalP and MglBAC, while intracellular Gal also leads to lower cAMP levels (reviewed in refs 58, 59).

The addition of Rib also resulted in an overall less YFP expression at 10 mM (Figure 5A). However, in contrast to the other sugars tested, this was not due to a major change in promoter kinetics (Figure 5C and Figure S3D). The peak of YFP expression was shifted for approximately 10 min, but the observed difference in the overall response was clearly due to differences in the YFP production rate (Figure S3D). Interestingly, the drop in module activity after the first peak, which was observed upon supplementation of 2 mM and 10 mM for the other sugars investigated, was completely absent in the case of Rib (compare Figure S3D to Figure S3A−C.. This suggests that in contrast to the other sugars, the addition of Rib did not reduce the intracellular cAMP levels and that the activation of P*lsrA* by cAMP-CRP remained possible. The slight but significant reduction of the module response at 10 mM Rib might be therefore rather due to an inhibition of the uptake of AI-2, which may indicate that in *E. coli*, AI-2 and Rib may compete for RbsB binding, similar to what was described for *Actinobacillus actinomycetemcomitans*.[2,60] Overall, the simple analysis of the kinetics of module induction can give a clear indication of whether the calculated AI-2 concentration was valid or if sugar was interfering with the measurement. However, as the actual P*lsrA* induction time points can slightly differ between experiments, it is necessary to include appropriate controls, e.g., synthetic DPD without sugar supplementation, when screening for residual sugars.

Analysis of the Kinetics of AI-2 Production in Mixed Bacterial Cultures. Xavier and Bassler showed that *E. coli* is able to import AI-2 produced by *V. harveyi*, and *V. harveyi* produces bioluminescence in response to *E. coli*-generated AI-2 during coculture experiments.[11] Therefore, we decided to test if our biosensor strain *E. coli* Δ*luxS* (*attB*::P*lsrA-yfp*) is suitable to analyze AI-2 production by a set of Gram-negative bacteria over time in coculture experiments (Figure 6). Additionally, we have tested the assay protocol with the Gram-positive bacterium *Staphylococcus aureus* 7.1 (*S. aureus*) (Figure S4).

We mixed *E. coli* Δ*luxS* (*attB*::P*lsrA-yfp*) with the bacteria of interest in a one-to-one ratio and measured the optical density and YFP expression over time. For *E. coli*, YFP expression was induced after around 300 min of coculture (Figure 6A), and the promoter induction peaked after ∼480 min. The kinetics of YFP expression induction by using *E. coli* Δ*luxS* (*attB*::P*lsrA-yfp*) mirrored the beginning of extracellular AI-2 accumulation and eventually the uptake via the unspecific PTS-dependent AI-2 transport[26] as indicated by a relatively flat slope from 300 to 400 min (Figure 6A). The subsequent expression of the AI-2-specific Lsr-ABC-transporter[16−18] then most likely resulted in a rapid uptake of AI-2, as judged by the steep incline of YFP expression induction until the total YFP amount reached the maximum after ∼480 min, as judged by the fluorescence signal. This revealed the functionality of our module during coculture regarding AI-2-dependent crosstalk between *E. coli* Δ*luxS* (*attB*::P*lsrA-yfp*) and its counterpart *E. coli*.

Next, we tested cocultures with the Gram-negative bacteria *Shigella flexneri* RKI 07-4792 (*S. flexneri*), *Proteus mirabilis* 532/04 (*P. mirabilis*), *Citrobacter koseri* isolate ATCC BAA895 (*C. koseri*), *Klebsiella pneumoniae* 52145 (*K. pneumoniae*), *Klebsiella aerogenes* 64 (*K. aerogenes*), and *Salmonella enterica* sv. Typhimurium isolate ATCC 14028 (*S.* Typhimurium). We saw AI-2-dependent YFP expression during coculture with *S. flexneri*, *C. koseri*, *K. pneumoniae*, and *K. aerogenes* (Figure 6B,D−F). In all cases, YFP expression was induced after around 300 min of coculture, supporting earlier studies that showed that the *lsrA* promoter is repressed in the early growth stages in LB broth due to catabolite repression.[17,20,21]

The coculture with the *C. koseri*, *K. aerogenes*, and *K. pneumoniae* isolates showed similar kinetics to the coculture with *E. coli* (compare Figure 6A to Figure 6D−F). Upon induction, the RFU slowly increased followed by a steep incline until the promoter induction peaked after ∼470−480 min of coculture with *C. koseri* and with *K. aerogenes* and after ∼500−520 min of coculture with *K. pneumonia* (Figure 6D−F). During coculture with *S. flexneri*, the kinetics did not show a two-phase RFU increase but a direct steep incline until the promoter induction peaked after ∼400−420 min (Figure 6B).

https://doi.org/10.1021/acssynbio.1c00459
ACS Synth. Biol. 2022, 11, 747−759

The reason for this lack of a two-phase expression pattern remains to be elucidated.

Coculture with *P. mirabilis* and *S.* Typhimurium did not lead to YFP expression (Figure 6C,G). We hypothesized that the absence of P*lsrA* induction might be caused by three possible reasons. First, *P. mirabilis* and/or *S.* Typhimurium might have killed *E. coli* by, e.g., microcin secretion (ref 61 reviewed in refs 62, 63). Second, we saw that *P. mirabilis* and *S.* Typhimurium have a faster growth rate in monoculture than *E. coli* (Figure S5), which could have resulted in an outgrowth of *E. coli* reporter cells. In the latter case, the lack of YFP expression may therefore be due to AI-2 self-uptake prior to the ability of *E. coli* to induce the *lsr* operon because of catabolite repression.[17,20,21] Third, there was the possibility that *P. mirabilis* and *S.* Typhimurium used in this study do not secrete AI-2 after all. To test our hypotheses, we checked for bacterial viability after 24 h of coculture. It was shown that different murine *P. mirabilis* isolates were able to kill murine *E. coli* isolates in coculture in the early stationary phase by using a contact-dependent killing system.[61] The viability assay revealed that *P. mirabilis* was able to kill *E. coli* (data not shown), as no living *E. coli* could be recovered from overnight cocultures. However, after 24 h of coculture with *S.* Typhimurium, the viability assay showed that a detectable but much lower number of *E. coli* cells were present in the overnight cultures (data not shown). Therefore, a potential incompatibility of bacteria for growth in cocultures has definitely to be taken into consideration and is limiting the analysis of real-time AI-2 production in cocultures with our biosensor strain *E. coli* Δ*luxS* (*attB*::P*lsrA-yfp*). During the cocultures with *E. coli*, *S. flexneri*, *C. koseri*, *K. pneumoniae*, and *K. aerogenes*, the promoter was induced after around 300 min, leading us to the assumption that after this time span, the catabolite repression is absent. Next, P*lsrA* induction is, in line with cAMP-CRP levels, specifically dependent on AI-2 (compare Figure 3).[17,20,21] Since the AI-2-dependent YFP expression increased for up to 2 h beginning at this time point (compare Figure 6B,D−F), we hypothesized that at the time point of P*lsrA* induction, the bacterial strains that we tested had produced AI-2. Thus, the extracellular AI-2 concentration should be measurable. Therefore, we sampled cell-free supernatants during monoculture after 5 h, 6 h, and 7 h of growth and measured extracellular AI-2 by using *E. coli* Δ*luxS* (pMK1) according to our protocol. We chose the same time points for *P. mirabilis* and *S.* Typhimurium since outgrowth or killing of *E. coli* should not affect extracellular AI-2. We saw maximal AI-2 activity in cell-free supernatants of monocultures of *E. coli*, *S. flexneri*, *P. mirabilis*, and *C. koseri* after 6 h of growth (Figure 6H−K). *For K. pneumoniae*, we saw high AI-2 activity after 5 h of growth, so we also isolated the cell-free supernatant after 4 h of growth (Figure 6L). Consequently, we saw that *K. pneumoniae* had produced AI-2 maximally after 5 h of monoculture (Figure 6L). Since AI-2 activity was low during 5−7 h of monoculture of *K. aerogenes* and *S.* Typhimurium, we chose to analyze cell-free supernatants after 3 h and 4 h of growth (Figure 6M,N). Subsequently, we saw that both bacteria had produced maximal AI-2 after 4 h of monoculture (Figure 6M,N). In summary, the real-time analysis can be a beneficial experiment to determine both the capability of bacteria to secrete AI-2 and an estimate of the time span of AI-2 secretion. Notably, if only one Gram-negative species should be analyzed, it might also be possible to use pMK1 directly in the heterogeneous host, depending on the compatibility of plasmid origin and promoter usage.

Analysis of the Extracellular AI-2 Concentration. While the coculture kinetics serves as a pre-experiment to determine (i) the capability of bacteria to produce AI-2 and (ii) the time point of maximal extracellular AI-2 concentration, the measurement of the exact concentration of the signaling molecule is not feasible in real-time experiments. This is because, during growth, AI-2 accumulates in the supernatant and is gradually internalized by the reporter strain. Additionally, also, the test strain internalizes AI-2. Therefore, the absolute quantification required cell-free supernatant sampling optimally after analyzing the AI-2 kinetics as described above.

In line with that, we calculated AI-2 concentrations in cell-free supernatants of *P. mirabilis*, *C. koseri*, *K. aerogenes*, *S.* Typhimurium, *S. flexneri*, and *K. pneumoniae*. The strains were grown in LB broth, and we sampled cell-free supernatants at the time points where we found the highest extracellular AI-2 activity during coculture (compare Figure 6H−N), which was after 6 h of growth of *E. coli*, *P. mirabilis*, *S. flexneri*, and *C. koseri*, after 5 h of growth of *K. pneumoniae*, and after 4 h of growth of *K. aerogenes* and *S.* Typhimurium. To keep test and control samples as comparable as possible, synthetic DPD was dissolved in sterile-filtered *E. coli* Δ*luxS* supernatant (after 6 h of growth) for the calibration curves (Figure S6). In the subsequent assay, the biosensor strain *E. coli* Δ*luxS* (pMK1) was used. The results are shown in Figure 7.

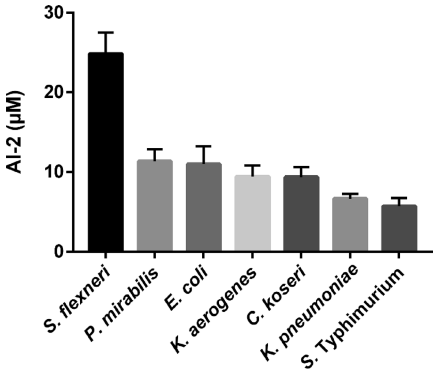

Figure 7. Quantification of AI-2 production by different enterobacterial isolates. Biologically active AI-2 concentrations in bacterial cell-free supernatants after 6 h of growth (*S. flexneri*, *P. mirabilis*, *E. coli*, and *C. koseri*), 5 h of growth (*K. pneumoniae*), or 4 h of growth (*K. aerogenes* and *S.* Typhimurium). Sample volumes were 50 μL in each case. The total assay volume was 200 μL. The biosensor strain used was *E. coli* Δ*luxS* (pMK1). Error bars represent three biological replicates with three technical replicates each.

After 6 h of growth, *E. coli* and *P. mirabilis* cultures had both reached an AI-2 concentration of ∼12 μM, and *C. koseri* cultures had reached an AI-2 concentration of ∼9 μM. Cultures of *S. flexneri*, on the other hand, had reached an AI-2 concentration of ∼24 μM, which is, by far, the highest AI-2 concentration when compared to the other bacterial strains. *K. pneumoniae* had reached an AI-2 concentration of ∼7 μM after 5 h of growth, and *K. aerogenes* cultures had reached an AI-2 concentration of ∼9 μM after 4 h of growth. *S.* Typhimurium had reached an AI-2 concentration of ∼5.5 μM after 4 h of growth, which was the lowest AI-2 concentration of all strains analyzed (Figure 7).

https://doi.org/10.1021/acssynbio.1c00459
ACS Synth. Biol. 2022, 11, 747−759

Thus, with the use of a calibration curve, the concentration of secreted biologically active AI-2 in the culture supernatants of Gram-negative bacteria (Figure 7) and *S. aureus* (Figure S7) can easily be quantified with the help of our reporter module. The AI-2 concentrations measured here were in the range in between 5.5 and 24 μM. However, also much higher AI-2 concentrations were already reported for culture supernatants of other bacteria. For example, AI-2 concentrations of ∼42 μM were reported for *Campylobacter jejuni* 81116AI2$^+$,[64] and AI-2 concentrations of up to 108 μM were reported for *Enterococcus faecalis* V583ΔABC.[65] These relatively high concentrations of AI-2 are well in the range of AI-2 concentrations that could be quantified with our reporter system.

CONCLUSIONS

The existing AI-2 bioassays have limitations, including trace-element interference, limitation to borated AI-2, or time-intensive, complex, and multistep protocols (see above). The bioassay described here is versatile, shows a broad detection range, and is less sensitive to sugars. The latter can be detected by analyzing the reporter module kinetics, which is a major advantage in analyzing potential AI-2 concentrations in complex samples as compared to already established methods. In addition, the hands-on time of this assay is short, and a one-step sample addition with subsequent result obtainment is less prone to human error when compared to multiple-step protocols.[42]

Taken together, these features of our bioassay should open up versatile and interesting application opportunities for the analysis of AI-2-dependent quorum sensing in the future.

METHODS

Bacterial Strains. Bacterial strains used in this study are listed in Table S2. Briefly, for module construction, the *E. coli* K-12 strain MG1655 and the *E. coli* strain DH5α were used. For experiments, the *E. coli* K-12 strain MG1655 (*E. coli*), *Proteus mirabilis* 532/04 (*P. mirabilis*), *Citrobacter koseri* ATCC BAA-895 (*C. koseri*), *Klebsiella aerogenes* 64 (*K. aerogenes*), *Salmonella enterica* sv. Typhimurium ATCC 14028 (*S.* Typhimurium), *Shigella flexneri* RKI 07-4792 (*S. flexneri*), and *Klebsiella pneumoniae* 52145 (*K. pneumoniae*) were used. For the sake of improved readability, in the text, we solely used the species designation as shown in the parentheses.

Media, Culture Methods, and Chemicals. All bacterial strains were grown by default in a 1× lysogeny broth medium (LB, containing 10 g/L tryptone, 5 g/L yeast extract, and 5 g/L NaCl). For solid medium preparation, 1.5% (w/v) agar was added. When required, the medium was supplemented with an appropriate amount of antibiotics in the following concentrations: chloramphenicol, 12.5−25 μg/mL; ampicillin, 100 μg/mL; zeocin, 50 μg/mL. For plasmid construction, the chemically competent *E. coli* strain DH5α was used. For plasmid transformation, electrocompetent *E. coli* strains were used. Upon transformation, bacteria were regenerated in 2xYT medium (containing 16 g/L tryptone, 10 g/L yeast extract, and 5 g/L NaCl). Unless otherwise stated, strains were grown overnight on LB agar plates that contained appropriate antibiotics if needed. Single colonies were picked and grown overnight in 1 mL of LB broth at 37 °C and continuously shaken in an incubation shaker (Multitron, INFORS HT, Switzerland). For strains containing a plasmid, an appropriate amount of antibiotics was added for overnight culture generation but not during experiments.

Synthetic DPD was purchased from Rita Ventura's research group at ITQB-UNL (Oeiras, Portugal).[67] DPD synthesis was carried out as reported by Rita Ventura's research group.[32] The synthetic DPD concentration was 16.8 mM, and the molecule was subsequently diluted to working concentrations in sterile ddH_2O. All steps were carried out on ice.

Sugar stock solutions, i.e., D-(+)-glucose (Sigma Aldrich), D-(+)-mannose (Sigma Aldrich), D-(+)-galactose (Sigma Aldrich), and D-(−)-ribose (Sigma Aldrich), of 1 M were made by suspending the appropriate amount of sugar in ddH_2O with subsequent sterile filtration using 0.22 μm syringe filters (Millex-GP, Millipore). Sugars were diluted to working concentrations in sterile ddH_2O.

PCR/Genomic DNA Purification and Analysis. Prior to Sanger sequencing or cloning, all PCR products were purified using either a NucleoSpin Gel and PCR Clean-up kit (Macherey-Nagel, Düren, Germany) or a Wizard SV Gel and PCR Clean-Up System kit (Promega, Walldorf, Germany). Plasmids were isolated using a NucleoSpin Plasmid Mini kit (Macherey-Nagel). Chromosomal DNA was isolated using a QIAamp DNA Mini kit (QIAGEN, Hilden Germany). PCR, plasmid, or gDNA quantification was done using a spectrophotometer (NanoDrop 2000, Thermo Fisher Scientific, Schwerte, Germany). The correct size of amplicons was verified by agarose gel electrophoresis using agarose (Biozym, Hessisch Oldendorf, Germany) in 1× TAE buffer. The gels were run at 110−130 V for 40−60 min, dependent on the size and agar concentration (1−1.5%). The size was estimated by the use of a GeneRuler 1 kb DNA ladder (Thermo Fisher Scientific).

Used Plasmids, Oligonucleotides, and Protein Accession Numbers. Used plasmids and oligonucleotides are listed in Tables S3 and S4, and protein accession numbers are listed in Table S5.

Construction of the *E. coli* Δ*luxS* Mutant. The *luxS* deletion mutant to inhibit AI-2 generation was constructed using the Red/ET recombineering method[66] and the *E. coli* K-12 strain MG1655 harboring the pKD46 plasmid (*E. coli* (pKD46)). The *luxS* gene was replaced by a zeocin resistance cassette (*BleoR*) that was amplified with Q5 High-Fidelity DNA polymerase (New England Biolabs, Frankfurt/Main, Germany) using the oligonucleotides Rec_BleoR_MG_fwd/Rec_BleoR_MG_rev and pEM7/Zeo as a template. The replacement was confirmed by colony PCR with a GoTaq Green Master Mix (Promega) using oligonucleotides zeo-control-fw/CFT073_DeltaLuxS_CP_rev and subsequent Sanger sequencing of the obtained PCR products.

Construction of pMK1 and Biosensor Strains. The plasmid pMK1 was constructed by first generating an *lsrRK lsrA* promoter-*yfp* fusion reporter cassette. For this, in the *E. coli* strain MG1655, the *lsrACDBFG* operon was replaced by a YFP open reading frame coupled to a chloramphenicol resistance cassette (*cat*) by using the Red/ET recombineering method[66] in *E. coli* (pKD46), resulting in *E. coli* (*lsrA-G::yfp-cat*). The *yfp-cat* cassette was amplified with Phusion High-Fidelity DNA polymerase (New England Biolabs) using oligonucleotides LZP47/LZP48 and pMB54 as a template. The replacement was confirmed by colony PCR using primer pairs LZP49/PST7 and MC_99/LZP50, respectively. The correct and seamless P*lsrA-yfp* fusion was determined by Sanger sequencing of the PCR product obtained by the primer

https://doi.org/10.1021/acssynbio.1c00459
ACS Synth. Biol. 2022, 11, 747−759

pair LZP49/PST7. Next, the *lsrRK lsrA* promoter-*yfp* fusion reporter cassette was amplified with Q5 High-Fidelity DNA polymerase (New England Biolabs) using oligonucleotides LKRS_fwd/LZP50 and chromosomal DNA of *E. coli* (*lsrA-G*::*yfp-cat*) as a template. The obtained PCR product was cloned into the *Sma*I (New England Biolabs)-digested low-copy plasmid pWKS30 by using DNA T4 ligase (New England Biolabs), and the *E. coli* strain DH5*α* was chemically transformed with the ligation mix. Correct plasmids were confirmed by colony PCR with a GoTaq Green Master Mix (Promega) using primers pKD3_lsr_seq_3/pMB54_lsrRK_CP2_rev and subsequent Sanger sequencing of the obtained purified plasmid.

The obtained plasmid (pMK1) was used for electroporation of *E. coli* Δ*luxS* to generate the biosensor strain for subsequent analysis.

Construction of *E. coli* Δ*luxS* (*attB*::P*lsrA-yfp*). The *lsrRK lsrA* promoter-*yfp* fusion reporter cassette was amplified with Q5 High-Fidelity DNA polymerase (New England Biolabs) using primers pWKS30_attB_fwd/pWKS30_attB_rev and pMK1 as a template. The obtained PCR product was inserted into the phage *λ attB* integration site (reviewed in ref 46) of the *E. coli* chromosome by using the Red/ET recombineering method[66] in *E. coli* Δ*luxS* (pKD46), resulting in *E. coli* Δ*luxS* (*attB*::P*lsrA-yfp*).

Brief AI-2 Bioassay Protocol. A step-by-step assay protocol is provided in the Supporting Information. Briefly, an overnight culture of the chosen Δ*luxS* mutant strain harboring either pMK1 or *attB*::P*lsrA-yfp* and an overnight culture of the Δ*luxS* mutant strain not harboring the reporter cassette (bacteria control) were generated. Overnight cultures were diluted in 10 mL of fresh LB broth in a 50 mL Erlenmeyer flask to a final optical density (OD_{600}) of 0.004. For optical density determination, overnight cultures were diluted 1:10 in phosphate-buffered saline (PBS, containing 8 g/L NaCl, 0.2 g/L KCl, 1.42 g/L Na_2HPO_4, and 0.27 g/L KH_2PO_4, pH 7.4), and the optical density was measured using a UV/Vis spectrophotometer (Ultrospec 2100 pro, Amersham Bioscience, UK). Strains were grown at 37 °C and continuously shaken. The cultures were grown until they reached the midexponential growth phase at OD_{600} = 0.4−0.6. The culture was subsequently aliquoted into a 96-well plate suited for fluorescence signal detection (Microplate, 96 well, F-Form, black; Greiner Bio-One, Frickenhausen, Germany). After aliquoting, samples were added to the cells, and the plate was inserted into a fluorescence plate reader and incubated with the following attributes: 37 °C, shaking, and optical density/fluorescence measurement (as described below) every 10 min. One well was filled with a 200 μL total volume. Bacterial control and biosensor strain volumes were dependent on the sample volume. All mentioned concentrations refer to final concentrations within the final 200 μL total volume.

Fluorescence Signal Detection and OD_{600} Measurements. For the fluorescence signal detection and OD_{600} measurements, either a TECAN Infinite M NANO$^+$ plate reader (TECAN, Männedorf, Switzerland) or a TECAN Infinite F200 (TECAN, Männedorf, Switzerland) was used. The optical density was either measured at 595 ± 9 nm (M NANO$^+$) or 595 ± 10 nm (F200). The fluorescence signal was either measured using an excitation wavelength of 514 nm (±9 nm) and an emission wavelength of 550 nm (±20 nm) (M NANO$^+$) or using an excitation wavelength of 485 nm (±20 nm) and an emission wavelength of 535 nm (±25 nm) (F200).

Data Processing. A step-by-step data processing protocol is provided in the Supporting Information.

Briefly, the raw data was processed as follows. First, the optical densities of the measured kinetics were corrected for the blank control (LB broth) by subtraction (OD_{600}). Second, the fluorescence emission measurements of samples were corrected for the background autofluorescence of the bacterial control by subtraction. The relative fluorescence units (RFU) were calculated by dividing the corrected fluorescence emission measurement by the corrected optical densities. To calculate the promoter activity, the derivative of RFU was calculated. For graphical depiction, negative derivative values were set to be zero. Next, the area under the curve (AUC) of the promoter activity was calculated (GraphPad Prism v7.0.0; San Diego, USA), and the maximal AUC of every kinetics was determined. For an easier comparison of the calculated AUC, the relative AUC (rel. AUC) was calculated by dividing the sample AUC by the indicated control AUC.

Coculture Assay Protocol. Overnight cultures of *E. coli* Δ*luxS* (*attB*::P*lsrA-yfp*), *E. coli* Δ*luxS*, and of the bacteria of interest were generated as described. Cultures were diluted to a final OD_{600} of 0.004 as described. Next, the diluted cultures were mixed in a 1:1 ratio and aliquoted in a total volume of 200 μL into a 96-well plate suited for fluorescence signal detection. In each experiment, the following mixtures were added: bacteria of interest + *E. coli* Δ*luxS* (*attB*::P*lsrA-yfp*) and, as controls, bacteria of interest + bacteria of interest and bacteria of interest + *E. coli* Δ*luxS*. The microplate was incubated with the following attributes: 37 °C, shaking, and optical density/fluorescence measurement every 10 min. RFU and RFU $f(x)^{-1}$ were measured as described in the detailed protocol. Notably, for the coculture assay, bacterial overnight cultures were used that expressed a low but detectable amount of the YFP. The initial cell density in the coculture experiments (dilution factor of <1:1.000 for each bacterial strain) was so low that the RFUs calculated for the initial time points of the experiments (up to approximately 200 min) are unreliable.

Calculation of AI-2 in Bacterial Cell-Free Medium. Overnight cultures were generated as described. The cultures were diluted to an OD_{600} of 0.004 in 10 mL of fresh LB broth in a 50 mL Erlenmeyer flask and incubated with continuous shaking at 180 rpm at 37 °C. For results in Figure 7, a cell-free bacterial medium was generated after 6 (*E. coli*, *P. mirabilis*, *S. flexneri*, and *C. koseri*), 5 (*K. pneumoniae*), or 4 h (*K. aerogenes* and *S.* Typhimurium) of growth. For results in Figure 6, a cell-free bacterial medium was generated after 5, 6, and 7 h (every strain) as well as after 3 h (*K. aerogenes* and *S.* Typhimurium) and after 4 h (*K. aerogenes*, *S.* Typhimurium, and *K. pneumoniae*) of growth. Aliquots of the cultures were centrifuged at 10,000*g* for 5 min, and the supernatant was used as samples. The cell-free medium was stored at 4 °C for a maximum of 24 h.

■ ASSOCIATED CONTENT

Supporting Information

The Supporting Information is available free of charge at https://pubs.acs.org/doi/10.1021/acssynbio.1c00459.

Detailed assay protocol; detailed data processing protocol; (Table S1) advantages and disadvantages of already established AI-2/BAI-2 quantification methods;

https://doi.org/10.1021/acssynbio.1c00459
ACS Synth. Biol. 2022, 11, 747−759

(Tables S2−S4) bacterial strains, plasmids, oligonucleotides, and protein accession numbers; (Figure S1) promoter activity upon addition of synthetic DPD to *E. coli* Δ*luxS* (pMK1); (Figure S2) biological replicates of dose−response curves; (Figure S3) impact of sugar on *lsrA* promoter activity; (Figure S4) comparison of AI-2 production kinetics by *Staphylococcus aureus* 7.1; (Figure S5) growth curves of *E. coli*, *P. mirabilis*, and *S.* Typhimurium; (Figure S6) dose−response curve for AI-2 quantification in bacterial supernatant; (Figure S7) quantification of AI-2 production by *Staphylococcus aureus* 7.1 (PDF)

AUTHOR INFORMATION

Corresponding Authors

Ulrich Dobrindt − *Institute of Hygiene, University of Münster, Münster 48149, Germany*; Email: dobrindt@uni-muenster.de

Michael Berger − *Institute of Hygiene, University of Münster, Münster 48149, Germany*; orcid.org/0000-0002-6480-1494; Email: michael.berger@ukmuenster.de

Author

Marla Keizers − *Institute of Hygiene, University of Münster, Münster 48149, Germany*; orcid.org/0000-0002-4954-6042

Complete contact information is available at: https://pubs.acs.org/10.1021/acssynbio.1c00459

Author Contributions

All authors have given approval to the final version of the manuscript. M.K., U.D., and M.B. performed conceptualization; M.K. performed experiments and data analysis; M.K. wrote the original draft; U.D. and M.B. rewrote and edited the manuscript; M.B. directly supervised the study; U.D. acquired funding.

Notes

The authors declare no competing financial interest.

ACKNOWLEDGMENTS

We thank A. Fruth (Robert Koch Institute, Wernigerode branch) for providing the *S. flexneri* isolate RKI 07-4792. This work was supported by the German Research Foundation (grant no. 281125614/GRK2220, EvoPAD project A3).

ABBREVIATIONS

AI-2, autoinducer-2; *V. harveyi*, *Vibrio harveyi*; *E. coli*, *Escherichia coli*; YFP, yellow fluorescent protein; AUC, area under the curve; Glc, D-(+)-glucose; Gal, D-(+)-galactose; Man, D-(+)-mannose; Rib, D-(−)-ribose; BAI-2, borated autoinducer-2

REFERENCES

(1) Fuqua, W. C.; Winans, S. C.; Greenberg, E. P. Quorum sensing in bacteria: the LuxR-LuxI family of cell density-responsive transcriptional regulators. *J. Bacteriol.* **1994**, *176*, 269−275.

(2) Pereira, C. S.; Thompson, J. A.; Xavier, K. B. AI-2-mediated signalling in bacteria. *FEMS Microbiol. Rev.* **2013**, *37*, 156−181.

(3) Taga, M. E.; Bassler, B. L. Chemical communication among bacteria. *Proc. Natl. Acad. Sci. U. S. A.* **2003**, *100*, 14549−14554.

(4) Bassler, B. L.; Greenberg, E. P.; Stevens, A. M. Cross-species induction of luminescence in the quorum-sensing bacterium Vibrio harveyi. *J. Bacteriol.* **1997**, *179*, 4043−4045.

(5) Zhang, L.; Li, S.; Liu, X.; Wang, Z.; Jiang, M.; Wang, R.; Xie, L.; Liu, Q.; Xie, X.; Shang, D.; Li, M.; Wei, Z.; Wang, Y.; Fan, C.; Luo, Z.-Q.; Shen, X. Sensing of autoinducer-2 by functionally distinct receptors in prokaryotes. *Nat. Commun.* **2020**, *11*, 5371.

(6) Schauder, S.; Shokat, K.; Surette, M. G.; Bassler, B. L. The LuxS family of bacterial autoinducers: biosynthesis of a novel quorum-sensing signal molecule. *Mol. Microbiol.* **2001**, *41*, 463−476.

(7) Sun, J.; Daniel, R.; Wagner-Döbler, I.; Zeng, A.-P. Is autoinducer-2 a universal signal for interspecies communication: a comparative genomic and phylogenetic analysis of the synthesis and signal transduction pathways. *BMC Evol Biol* **2004**, *4*, 36.

(8) Chen, X.; Schauder, S.; Potier, N.; Van Dorsselaer, A.; Pelczer, I.; Bassler, B. L.; Hughson, F. M. Structural identification of a bacterial quorum-sensing signal containing boron. *Nature* **2002**, *415*, 545−549.

(9) Miller, S. T.; Xavier, K. B.; Campagna, S. R.; Taga, M. E.; Semmelhack, M. F.; Bassler, B. L.; Hughson, F. M. Salmonella typhimurium recognizes a chemically distinct form of the bacterial quorum-sensing signal AI-2. *Mol. Cell* **2004**, *15*, 677−687.

(10) Meijler, M. M.; Hom, L. G.; Kaufmann, G. F.; McKenzie, K. M.; Sun, C.; Moss, J. A.; Matsushita, M.; Janda, K. D. Synthesis and biological validation of a ubiquitous quorum-sensing molecule. *Angew. Chem., Int. Ed.* **2004**, *43*, 2106−2108.

(11) Xavier, K. B.; Bassler, B. L. Interference with AI-2-Mediated Bacterial Cell-Cell Communication. *Nature* **2005**, *437*, 750−753.

(12) Papenfort, K.; Bassler, B. L. Quorum sensing signal-response systems in Gram-negative bacteria. *Nat Rev Microbiol* **2016**, *14*, 576−588.

(13) Tavender, T. J.; Halliday, N. M.; Hardie, K. R.; Winzer, K. LuxS-independent formation of AI-2 from ribulose-5-phosphate. *BMC Microbiol* **2008**, *8*, 98.

(14) Ismail, A. S.; Valastyan, J. S.; Bassler, B. L. A Host-Produced Autoinducer-2 Mimic Activates Bacterial Quorum Sensing. *Cell Host Microbe* **2016**, *19*, 470−480.

(15) Bassler, B. L.; Wright, M.; Silverman, M. R. Multiple signalling systems controlling expression of luminescence in Vibrio harveyi: sequence and function of genes encoding a second sensory pathway. *Mol. Microbiol.* **1994**, *13*, 273−286.

(16) Taga, M. E.; Semmelhack, J. L.; Bassler, B. L. The LuxS-dependent autoinducer AI-2 controls the expression of an ABC transporter that functions in AI-2 uptake in Salmonella typhimurium. *Mol. Microbiol.* **2001**, *42*, 777−793.

(17) Xavier, K. B.; Bassler, B. L. Regulation of uptake and processing of the quorum-sensing autoinducer AI-2 in Escherichia coli. *J. Bacteriol.* **2005**, *187*, 238−248.

(18) Pereira, C. S.; de Regt, A. K.; Brito, P. H.; Miller, S. T.; Xavier, K. B. Identification of functional LsrB-like autoinducer-2 receptors. *J. Bacteriol.* **2009**, *191*, 6975−6987.

(19) Taga, M. E.; Miller, S. T.; Bassler, B. L. Lsr-mediated transport and processing of AI-2 in Salmonella typhimurium. *Mol. Microbiol.* **2003**, *50*, 1411−1427.

(20) Wang, L.; Li, J.; March, J. C.; Valdes, J. J.; Bentley, W. E. luxS-Dependent Gene Regulation in Escherichia coli K-12 Revealed by Genomic Expression Profiling. *J. Bacteriol.* **2005**, *187*, 8350−8360.

(21) Wang, L.; Hashimoto, Y.; Tsao, C.-Y.; Valdes, J. J.; Bentley, W. E. Cyclic AMP (cAMP) and cAMP receptor protein influence both synthesis and uptake of extracellular autoinducer 2 in Escherichia coli. *J. Bacteriol.* **2005**, *187*, 2066−2076.

(22) Shao, H.; James, D.; Lamont, R. J.; Demuth, D. R. Differential interaction of Aggregatibacter (Actinobacillus) actinomycetemcomitans LsrB and RbsB proteins with autoinducer 2. *J. Bacteriol.* **2007**, *189*, 5559−5565.

(23) Armbruster, C. E.; Pang, B.; Murrah, K.; Juneau, R. A.; Perez, A. C.; Weimer, K. E. D.; Swords, W. E. RbsB (NTHI_0632) mediates quorum signal uptake in nontypeable Haemophilus influenzae strain 86-028NP. *Mol. Microbiol.* **2011**, *82*, 836−850.

(24) Fitts, E. C.; Andersson, J. A.; Kirtley, M. L.; Sha, J.; Erova, T. E.; Chauhan, S.; Motin, V. L.; Chopra, A. K. New Insights into Autoinducer-2 Signaling as a Virulence Regulator in a Mouse Model of Pneumonic Plague. *mSphere* **2016**, *1*, No. e00342-16.

(25) Kamaraju, K.; Smith, J.; Wang, J.; Roy, V.; Sintim, H. O.; Bentley, W. E.; Sukharev, S. Effects on membrane lateral pressure suggest permeation mechanisms for bacterial quorum signaling molecules. *Biochemistry* **2011**, *50*, 6983−6993.
(26) Pereira, C. S.; Santos, A. J. M.; Bejerano-Sagie, M.; Correia, P. B.; Marques, J. C.; Xavier, K. B. Phosphoenolpyruvate phosphotransferase system regulates detection and processing of the quorum sensing signal autoinducer-2. *Mol. Microbiol.* **2012**, *84*, 93−104.
(27) Marques, J. C.; Oh, I. K.; Ly, D. C.; Lamosa, P.; Ventura, M. R.; Miller, S. T.; Xavier, K. B. LsrF, a coenzyme A-dependent thiolase, catalyzes the terminal step in processing the quorum sensing signal autoinducer-2. *Proc. Natl. Acad. Sci. U. S. A.* **2014**, *111*, 14235−14240.
(28) Vilchez, R.; Lemme, A.; Thiel, V.; Schulz, S.; Sztajer, H.; Wagner-Döbler, I. Analysing traces of autoinducer-2 requires standardization of the Vibrio harveyi bioassay. *Anal. Bioanal. Chem.* **2007**, *387*, 489−496.
(29) Rickard, A. H.; Campagna, S. R.; Kolenbrander, P. E. Autoinducer-2 is produced in saliva-fed flow conditions relevant to natural oral biofilms. *J Appl Microbiol* **2008**, *105*, 2096−2103.
(30) Rui, F.; Marques, J. C.; Miller, S. T.; Maycock, C. D.; Xavier, K. B.; Ventura, M. R. Stereochemical diversity of AI-2 analogs modulates quorum sensing in Vibrio harveyi and Escherichia coli. *Bioorg. Med. Chem.* **2012**, *20*, 249−256.
(31) Yu, J.; Madsen, M. L.; Carruthers, M. D.; Phillips, G. J.; Kavanaugh, J. S.; Boyd, J. M.; Horswill, A. R.; Minion, F. C. Analysis of Autoinducer-2 Quorum Sensing in Yersinia pestis. *Infect. Immun.* **2013**, *81*, 4053−4062.
(32) Ascenso, O. S.; Marques, J. C.; Santos, A. R.; Xavier, K. B.; Ventura, M. R.; Maycock, C. D. An efficient synthesis of the precursor of AI-2, the signalling molecule for inter-species quorum sensing. *Bioorg. Med. Chem.* **2011**, *19*, 1236−1241.
(33) DeKeersmaecker, S. C. J.; Vanderleyden, J. Constraints on detection of autoinducer-2 (AI-2) signalling molecules using Vibrio harveyi as a reporter. *Microbiology (Reading)* **2003**, *149*, 1953−1956.
(34) Turovskiy, Y.; Chikindas, M. L. Autoinducer-2 bioassay is a qualitative, not quantitative method influenced by glucose. *J. Microbiol. Methods* **2006**, *66*, 497−503.
(35) Henke, J. M.; Bassler, B. L. Three parallel quorum-sensing systems regulate gene expression in Vibrio harveyi. *J. Bacteriol.* **2004**, *186*, 6902−6914.
(36) Long, T.; Tu, K. C.; Wang, Y.; Mehta, P.; Ong, N. P.; Bassler, B. L.; Wingreen, N. S. Quantifying the Integration of Quorum-Sensing Signals with Single-Cell Resolution. *PLoS Biol.* **2009**, *7*, No. e1000068.
(37) Tu, K. C.; Bassler, B. L. Multiple small RNAs act additively to integrate sensory information and control quorum sensing in Vibrio harveyi. *Genes Dev.* **2007**, *21*, 221−233.
(38) Rajamani, S.; Zhu, J.; Pei, D.; Sayre, R. A LuxP-FRET-based reporter for the detection and quantification of AI-2 bacterial quorum-sensing signal compounds. *Biochemistry* **2007**, *46*, 3990−3997.
(39) Taga, M. E.; Xavier, K. B. Methods for analysis of bacterial autoinducer-2 production. *Curr Protoc Microbiol Chapter* **2011**, *1*, 1C.
(40) Zhu, J.; Pei, D. A LuxP-based fluorescent sensor for bacterial autoinducer II. *ACS Chem. Biol.* **2008**, *3*, 110−119.
(41) Roy, V.; Smith, J. A. I.; Wang, J.; Stewart, J. E.; Bentley, W. E.; Sintim, H. O. Synthetic analogs tailor native AI-2 signaling across bacterial species. *J. Am. Chem. Soc.* **2010**, *132*, 11141−11150.
(42) Ilina, P.; Ma, X.; Sintim, H. O.; Tammela, P. Miniaturized whole-cell bacterial bioreporter assay for identification of quorum sensing interfering compounds. *J. Microbiol. Methods* **2018**, *154*, 40−45.
(43) Mok, K. C.; Wingreen, N. S.; Bassler, B. L. Vibrio harveyi quorum sensing: a coincidence detector for two autoinducers controls gene expression. *EMBO J* **2003**, *22*, 870−881.
(44) Drees, B.; Reiger, M.; Jung, K.; Bischofs, I. B. A Modular View of the Diversity of Cell-Density-Encoding Schemes in Bacterial Quorum-Sensing Systems. *Biophys. J.* **2014**, *107*, 266−277.
(45) Schaefer, J.; Jovanovic, G.; Kotta-Loizou, I.; Buck, M. Single-step method for β-galactosidase assays in Escherichia coli using a 96-well microplate reader. *Anal. Biochem.* **2016**, *503*, 56−57.
(46) Campbell, A. M. Chromosomal insertion sites for phages and plasmids. *J. Bacteriol.* **1992**, *174*, 7495−7499.
(47) Berger, M.; Gerganova, V.; Berger, P.; Rapiteanu, R.; Lisicovas, V.; Dobrindt, U. Genes on a Wire: The Nucleoid-Associated Protein HU Insulates Transcription Units in Escherichia coli. *Sci. Rep.* **2016**, *6*, 31512.
(48) Xue, T.; Zhao, L.; Sun, H.; Zhou, X.; Sun, B. LsrR-binding site recognition and regulatory characteristics in Escherichia coli AI-2 quorum sensing. *Cell Res* **2009**, *19*, 1258−1268.
(49) Choi, J.; Shin, D.; Kim, M.; Park, J.; Lim, S.; Ryu, S. LsrR-Mediated Quorum Sensing Controls Invasiveness of Salmonella typhimurium by Regulating SPI-1 and Flagella Genes. *PLoS One* **2012**, *7*, No. e37059.
(50) Servinsky, M. D.; Terrell, J. L.; Tsao, C.-Y.; Wu, H.-C.; Quan, D. N.; Zargar, A.; Allen, P. C.; Byrd, C. M.; Sund, C. J.; Bentley, W. E. Directed assembly of a bacterial quorum. *ISME J* **2016**, *10*, 158−169.
(51) Stephens, K.; Zargar, A.; Emamian, M.; Abutaleb, N.; Choi, E.; Quan, D. N.; Payne, G.; Bentley, W. E. Engineering Escherichia coli for enhanced sensitivity to the autoinducer-2 quorum sensing signal. *Biotechnol. Prog.* **2019**, *35*, No. e2881.
(52) Ha, J.-H.; Hauk, P.; Cho, K.; Eo, Y.; Ma, X.; Stephens, K.; Cha, S.; Jeong, M.; Suh, J.-Y.; Sintim, H. O.; Bentley, W. E.; Ryu, K.-S. Evidence of link between quorum sensing and sugar metabolism in Escherichia coli revealed via cocrystal structures of LsrK and HPr. *Sci Adv 4*, eaar7063. 2018.
(53) Bodor, A. M.; Jänsch, L.; Wissing, J.; Wagner-Döbler, I. The luxS mutation causes loosely-bound biofilms in Shewanella oneidensis. *BMC Res Notes* **2011**, *4*, 180.
(54) Wang, T.-N.; Kaksonen, A. H.; Hong, P.-Y. Evaluation of two autoinducer-2 quantification methods for application in marine environments. *J Appl Microbiol* **2018**, *124*, 1469−1479.
(55) Deutscher, J.; Francke, C.; Postma, P. W. How phosphotransferase system-related protein phosphorylation regulates carbohydrate metabolism in bacteria. *Microbiol Mol Biol Rev* **2006**, *70*, 939−1031.
(56) Liu, X.; Zeng, J.; Huang, K.; Wang, J. Structure of the mannose transporter of the bacterial phosphotransferase system. *Cell Res* **2019**, *29*, 680−682.
(57) Görke, B.; Stülke, J. Carbon catabolite repression in bacteria: many ways to make the most out of nutrients. *Nat Rev Microbiol* **2008**, *6*, 613−624.
(58) Weickert, M. J.; Adhya, S. The galactose regulon of Escherichia coli. *Mol. Microbiol.* **1993**, *10*, 245−251.
(59) Death, A.; Ferenci, T. Between feast and famine: endogenous inducer synthesis in the adaptation of Escherichia coli to growth with limiting carbohydrates. *J. Bacteriol.* **1994**, *176*, 5101−5107.
(60) James, D.; Shao, H.; Lamont, R. J.; Demuth, D. R. The Actinobacillus actinomycetemcomitans ribose binding protein RbsB interacts with cognate and heterologous autoinducer 2 signals. *Infect. Immun.* **2006**, *74*, 4021−4029.
(61) Kiani, D.; Santus, W.; Kiernan, K. A.; Behnsen, J. Proteus mirabilis Employs a Contact-Dependent Killing System against Competing Enterobacteriaceae. *mSphere* **2021**, No. e0032121.
(62) Vriezen, J. A. C.; Valliere, M.; Riley, M. A. The evolution of reduced microbial killing. *Genome Biol Evol* **2009**, *1*, 400−408.
(63) Hibbing, M. E.; Fuqua, C.; Parsek, M. R.; Peterson, S. B. Bacterial competition: surviving and thriving in the microbial jungle. *Nat Rev Microbiol* **2010**, *8*, 15−25.
(64) Plummer, P.; Zhu, J.; Akiba, M.; Pei, D.; Zhang, Q. Identification of a Key Amino Acid of LuxS Involved in AI-2 Production in Campylobacter jejuni. *PLoS One* **2011**, *6*, No. e15876.
(65) Rossmann, F. S.; Racek, T.; Wobser, D.; Puchalka, J.; Rabener, E. M.; Reiger, M.; Hendrickx, A. P. A.; Diederich, A.-K.; Jung, K.; Klein, C.; Huebner, J. Phage-mediated Dispersal of Biofilm and Distribution of Bacterial Virulence Genes Is Induced by Quorum Sensing. *PLoS Pathog.* **2015**, *11*, No. e1004653.

https://doi.org/10.1021/acssynbio.1c00459
ACS Synth. Biol. 2022, 11, 747−759

(66) Sharan, S. K.; Thomason, L. C.; Kuznetsov, S. G.; Court, D. L. Recombineering: a homologous recombination-based method of genetic engineering. *Nat. Protoc.* **2009**, *4*, 206−223.
(67) https://itqb.unl.pt/research/chemistry/bioorganic-chemistry

https://doi.org/10.1021/acssynbio.1c00459
ACS Synth. Biol. 2022, 11, 747−759